An integrated tsunami inundation and vulnerability analysis at the Makran Coast, Pakistan

Rashid Haider[1,3], Sajid Ali[1], Gösta Hoffmann[2], Klaus Reicherter[1]

[1] Institute of Neotectonics and Natural Hazards, RWTH Aachen University, Lochnerstr. 4-20, 52056 Aachen, Germany
[2] UNESCO Global Geoparks Unit, Department Heritage, Nature, Society, German Commission for UNESCO, Martin-Luther-Allee 42 53175 Bonn, Germany
[3] Geoscience Advanced Research Laboratories, Geological Survey of Pakistan, Islamabad 45500, Pakistan

Correspondence to: Rashid Haider (r.haider@nug.rwth-aachen.de)

Abstract. The coastal cities ~~and areas~~ of Gwadar and Pasni in the Arabian Sea, located in the northwest of the Indian Ocean, are investigated for inundation and vulnerability analysis. ~~For modelling, both dynamic and static approaches are used for better understanding and for their comparative analysis~~. ~~The~~ Maximum tsunami wave potential in the Arabian Sea is estimated through compiling and assessing the paleo-morphodynamics of tsunamites records found along its coastlines. Off these tsunamites, the one exhibiting the worst case is modelled to evaluate the maximum wave potential. ~~The dynamic model is calibrated and validated with the inundation limits of the 1945 tsunami in the Pasni area~~. ~~Further, for vulnerability estimation,~~ Based on the wave potential evaluation, three different wave scenarios (7 m, 10 m, and 15 m) are projected on Pasni and Gwadar and surrounding areas. Results show that both cities are highly vulnerable to wave heights ≥7 m and wave lengths ≥ 15 km. The 15 m scenario would be almost a complete disaster for both cities and adjoining towns. Moreover, ~~R~~results of simulation ~~and comparative analysis also~~ show that due to coastal orientation and morphology, the reflection, integration, and amplification phenomena have a devastating effect on the region, and their intensity increases with the increasing size of the approaching waveform. ~~It~~ The reflection-amplification phenomenon variably but significantly affects the inundation extents and depths. ~~At the end, b~~Based on the simulated results, the utility of the installed early warning system is also assessed.

1 Introduction

Tsunamis are rare events but have high damage potential for the coastal communities. In the past 27 years, 64 tsunamis with a run-up higher than 3 m have been documented globally (Tarbotton et al., 2015). In the recent two decades, there has been a substantial advancement in our understanding of tsunami formation, propagation, and inundation, enabling planners, administrators, and engineers to calibrate the building's design codes in order to mitigate the disaster risk (Park et al., 2013; Macintosh, 2013). In this regard, inundation analysis is an important tier in vulnerability and risk assessment. It is done by integrating the infrastructure's fragility curves (damage probability curves) with different tsunami-flow magnitudes (Rehman and Cho, 2016). These fragility curves are generated through various techniques based on engineering and statistical

approaches, while the tsunami-flow magnitude is a product of flow depth and flow velocity calculated through dynamic inundation modelling.

In this paper, two aspects have been investigated~~:~~: primarily the inundation analysis and secondarily a vulnerability estimation for the coastal cities of Pasni and Gwadar (see Fig. 1). These cities were worst affected by the 1945 earthquake (Mw 8.1) entailing tsunami which resulted in hundreds of casualties (Pendse, 1946; Hoffmann et al., 2013b). In 2013, a small tsunami (<1m) associated with an earthquake ~~(~~(Mw 7.7) struck the same area once more but caused no damage (Heidarzadeh and Satake, 2014b). Both cities had grown up many times as compared to those in 1945, and in the case of any such disaster, a huge life and property losses are expected. ~~Kakar et al. (2014) under the patronage of the UNESCO-Intergovernmental Oceanographic Commission (IOC), interviewed the eyewitnesses and survivors in the affected areas of Pakistan and neighbouring countries. Furthermore, interviewees named various inundated locations and extents in different areas. Based on these eyewitness accounts, the locations on a map and DEM were pinned up to find the inundation extent and run-up heights in the Pasni, Ormara, and Gwadar (Lodhi et al., 2021). In the follow-up studies; the Pasni was revisited to mark the inundation extents and to rectify some ambiguities in the map of Lodhi et al. (2021). We used survivor accounts and field evidence to map inundation extents of the 1945 Tsunami. Next, several tsunami scenarios are simulated to look for the one satisfying these inundation limits. Based on the results of the fieldwork, our models are validated.~~

~~The 1945 wave heights at Pasni are reported differently (Table 4). This is why we used 1945 runup heights measured in the field and simulated various scenarios to estimate the waveform(s) capable of demonstrating the 1945 scenario.~~

2 Tectonic settings and Associated Seismicity

The majority (80%) of tsunamis on the globe are caused by underwater earthquakes (Harbitz et al., 2014; Løvholt, 2017) , while the other 20% are brought on by landslides, volcanoes, and meteoric impacts in ocean water (Behrens et al., 2021). In the Arabian Sea, most of the seismic activity is attributed to the Makran Subduction Zone (MSZ). The MSZ accommodates the crustal shortening between the Arabian Plate in the south and the Eurasian Plate in the north, converging at a rate of 0.5–20 mm/year (Vernant et al., 2004; Khan et al., 2008; Jade et al., 2017). The majority of the seismicity along the eastern MSZ, south of Pasni, is attributable to the Sonne Fault (Kukowski et al., 2000). On the other hand, the high seismic velocities (4.4 km/s) suggest a brittle decollement at MSZ which is responsible for high seismicity (Smith et al., 2012). The lack of soft sediments in comparison to its western portion is what causes the brittle nature. The MSZ's thermal modelling shows that its potential is comparable to the December 2004 Sumatra rupture and could trigger up to a (Mw 9.2) earthquake (Smith et al., 2012). Estimates from a different thermal modelling research suggests a potential of Mw 8.65 ± 0.26 in western Makran (Iran) and 8.75 ± 0.26 in eastern Makran, Pakistan (Khaledzadeh and Ghods, 2022). El-Hussain et al. (2016) inversely calculated the maximum moment of earthquake as Mw 8.8 using the geodetic slip rate based on a simplified relation by Brune (1968), Hanks and Kanamori (1979).

The focal mechanism of the 1945 tsunamigenic earthquake shows that it is related to a thrust event (Byrne et al., 1992). The ruptured lengths predicted by their dislocation models, body waveform inversion, and moment estimations range from 100 to 200 km with an average 7 m slip of crust along the MSZ. The Arabian Plate, along with subducting its northern edge, slides past the Indian Plate at a rate of about 3±1 mm/yr (Reilinger et al., 2006; Rodriguez et al., 2011) making it an active transform plate boundary. Right-lateral strike-slip and normal faulting cause minor earthquakes to occur in the Murray Ridge (Banghar and Syke, 1981). The largest magnitude observed along the remaining OFZ is Mw 5.8, and the seismicity is likewise mild to moderate (Rodriguez et al., 2011), hence posing no major tsunami threat. An integrated tsunami hazard assessment using multiproxy proxy analysis shows a return period between 500-1000 years for a tsunami ≥ 10 m in the Arabian Sea (Haider et al., 2023).

3 Methods

~~3.1 Tsunami Modelling and Data Sets~~

~~Numerical modelling is performed using earthquake source parameters at MSZ using the Delft3D 4.04.01 software, developed by the Dutch Institute Deltares (Deltares, 2017). The hydrodynamic programme module Delft3D-FLOW is used for simulation, which solves non-linear 2D and 3D shallow water equations for unsteady flow phenomena. The shallow water equations (SWE) of the Boussinesq approximation for incompressible fluids are derived from the three-dimensional hydrodynamic Navier-Stokes equations as represented by water and are in good approximation. The Delft3D-FLOW module performs simulation calculations of tsunami waves using the two-dimensional, depth-averaged calculation method (for further details, please see Deltares 2012: 183–279).~~

~~We used a nested computational grid for both cities. The grid resolution for the nested models is 0.0004×0.0004 (44 m × 44 m) and 0.01 × 0.01 (~1 km × 1 km) for the regional model. A schematic nesting model is presented in Supplements: Simulations-10. In the regional model, Reinmann boundary conditions are used to minimise the reflection effect and time-series boundaries for the nested models. For tsunami propagation and inundation, the General Bathymetric Chart of the Oceans (GEBCO) 15 arc seconds and the German Aerospace Centre's (DLR) 0.4 arcsec (~12 m) DEM are fused together. DEM is produced from bistatic X-Band interferometric SAR data using the DLR's patented TanDEM-X and TerraSAR-X. The post-data acquisition developments are manually added to the fused DEM. These changes are significant for the Gwadar as the East Bay Express Way and jetty (4 m high each) are manually added to the DEM. There has been no significant change in the Pasni topography since 1945. A few 1945 tsunami survivors claim about the co-seismic subsidence (~2 m) at the NE part of the city. As of 2023, this subsided topography has almost been replenished by the beach sand accretion processes. However, the population density of the Pasni Town has considerably increased offering more surface resistance as compared to that in 1945. This increase hampers the results in the populated parts of the study area. To overcome this problem, inundation extent mapping and modeling mostly relies on the areas either still open or thinly populated.~~

~~Finally, the terrain roughness is assigned using Manning's Coefficient with values ranging as 0.015 sea floor and open land, 0.03 thinly populated areas, 0.05 moderately populated areas to 0.08 densely populated areas. The coefficient's assignment is based on fieldwork, photographs, and Google Earth Satellite Images.~~

3.1~~2~~ Tsunami Wave Assessment and Scenario Selection

In addition to the recorded tsunami wave height of 12-15 meters in 1945 at Pasni, the potential for tsunami waves in the Arabian Sea is assessed by utilizing the tsunamites proxy at Fin, Oman, (further details below).

We compiled the reported tsunamites cases ~~along with their displacements from the source due to extreme wave events~~ around the Arabian Sea and ~~took~~ specifically examined the case at Fins, Oman exhibiting extreme morphodynamics ~~situated at Fins, Oman~~ (Table S1 supplements). ~~Here~~At Fins, the tsunamites are represented by block and boulder deposits up to 40 tonnes lying at a maximum height of 10 m from the mean sea level (msl) showing a landward transportation ~~of a maximum~~upto 50 m from their intact sites. Further, laboratory tests on a scaled model (t-LiDAR) of the largest block estimated wave velocities for dislodging, elevating, and transporting these boulders to be between 4.5 and 6.6 meters per second (m/s) ~~For dislodging, elevating, and transporting, an estimated wave velocity of 4.5–6.6 m/s is computed~~ (Hoffmann et al., 2013a). The marine shells (C^{14}, n=4), attached to these blocks and boulders gave a wide range of age between 250±160 and 4595±185 cal. BP (Hoffmann et al., 2020). At the same site, loose tsunami sediments fining and wedging landward with a minimum elevation of ≥17 m is dated 5840 cal. BP (C^{14}, n=6) (Koster et al., 2014). They also applied corrections for tectonic uplift/subsidence, absolute sea level change and estimated a 14 m wave run-up. The long axis rose plot of blocks and boulders also points to the wave source of palaeocurrent (N30E) as the MSZ (Hoffmann et al., 2013a). We modelled this case study to estimate the wave size capable to demonstrate the above scenario.~~We simulated various scenarios at western MSZ and estimated that a 15 m high tsunami wave can have a maximum 5 m/s flow velocity with a maximum flow depth of 9 m at the cliff edge (Supplements: Simulations 1 Fins Sur, Oman).~~ The tsunamis is generated using OKHADA earthquake parameters at MSZ ~~is~~ given in table ~~---------~~ ~~(Mw 9.5, fault slip 15 m, width 200 km, depth 30 km, dip 7°)~~. The other tsunami sources have not yet been considered and therefore cannot be negated.

The 1945 tsunami at Pasni is also ~~taken as~~ a severe event in the known history of tsunamis in the Arabian Sea. The reported wave height of 1945 tsunami at Pasni is 12m ~~–~~ 15m (Pendse, 1946). ~~The inundation heights for this event were recorded during field work by tracing the localities pointed out by the survivors of the 1945 tsunami (Table 2). In the field work, the maximum elevation of inundation extent mapped was found to be 10 meters laying 1.6 km inland from mean sea level~~. ~~The reported wave height of 1945 tsunami is 12m – 15m (Pendse, 1946).~~

The 1945 tsunami event in Pasni and extreme morphodynamic case of tsunamites at Fins serves as a reference, providing empirical evidence of tsunami potential and its impacts within the region. The recurrence interval for a tsunami event of such magnitude (≥ 10 m) is estimated to be between 500 to 1000 years (Haider et al., 2023). ~~From these historical~~ Based on the above assessment, we establish a range of scenarios (7 m, 10 m, and 15 m) to thoroughly assess the vulnerability landscape

of Gwadar and Pasni cities and their surrounding areas.~~precedents, we derive a range of scenarios (7 m, 10 m, and 15 m) encompassing varying wave heights to comprehensively evaluate the vulnerability landscape of Gwadar and Pasni cities and surrounding areas~~.

3.~~3~~2 Source Type and Parameters

Tsunami scenarios are modeled using the earthquake parameters on ~~at MSZ and adjoining splay~~hypothetical splay fault close to MSZ~~s~~. ~~The relationship between earthquake magnitude and associated parameters is inherently complex, primarily due to the intricate nature of geological processes. This complexity necessitates comprehensive data collection and a deep understanding of geological phenomena~~. ~~However, we~~We employed the Okada's (1985) ~~-~~mathematical model~~, a widely used tool in seismology and tsunami research,~~ to estimate seabed deformation caused by earthquakes. The applied uniform fault parameters ~~are applied~~ to a four segmented fault rupture. The worst-case source parameters ~~(Mw 9.5)~~ were replicated from those tested in the western MSZ, specifically for the Fins case. ~~The initial wave height could potentially reach up to maximum 15 meters, indicating a significant risk of tsunami inundation~~. To enhance vulnerability assessment, we conducted two additional case studies with scenarios with relative low parameters ~~of Mw 8.5 and Mw 9.0~~ (Table---). These scenarios likely represent varying levels of seismic hazard and tsunami risk, enabling a more comprehensive evaluation of potential impacts and the development of effective mitigation strategies. The relationship between earthquake magnitude and associated parameters is inherently complex, primarily due to the intricate nature of geological processes such as complexity of fault geometry, heterogeneous stress distribution, and uncertainties in earthquake rupture processes (Zaccagnino et al., 2022).

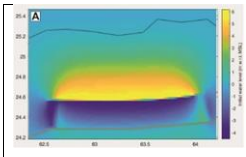

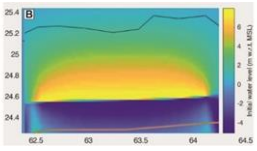

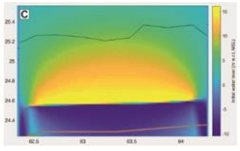

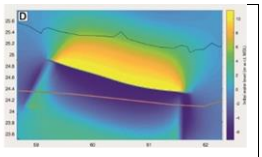

Length (km)	Strike (deg)	Width (km)	Depth (km)	Dip (deg)	Rake (deg)	Slip (m)	Initial Wave height
200	-84 to -70	211	10	35	90	22	D
200	266 to 269	211	10	35	90	22	C
200	266 to 269	160	10	35	90	10	B
200	266 to 269	110	10	35	90	8	A

3.3 Tsunami Modelling and Data Sets

Numerical modelling is performed using earthquake source parameters at MSZ conducted using the Delft3D 4.04.01 software, developed by the Dutch Institute Deltares (Deltares, 2017). The hydrodynamic programme module Delft3D-FLOW is used for simulation, which solves non-linear 2D and 3D shallow water equations for unsteady flow phenomena. The shallow water equations (SWE) of the Boussinesq approximation for incompressible fluids are derived from the three-dimensional hydrodynamic Navier-Stokes equations as represented by water and are in good approximation. The Delft3D-FLOW module performs simulation calculations of tsunami waves using the two-dimensional, depth-averaged calculation method (for further details, please see Deltares 2012: 183–279).

We utilized a nested computational grid for both cities, with the grid resolution set at 0.0004×0.0004 (44 m × 44 m) for the nested models and 0.01 × 0.01 (~1 km × 1 km) for the regional model. A schematic nesting model is presented in Supplements: Simulations-10. In the regional model, Reinmann Boundary Conditions are used to minimise the reflection effect and time-series boundaries for the nested models. For tsunami propagation and inundation, the General Bathymetric Chart of the Oceans (GEBCO) 15 arc seconds bathymetry and the German Aerospace Centre's (DLR) 0.4 arcsec (~12 m) topography are fused together in a GIS environment. The DLR's topography Digital Elevation Model (DEM) is derived from bistatic X-Band interferometric Synthetic Aperture Radar (SAR) data, employing the patented TanDEM-X and TerraSAR-X systems. The post-data acquisition developments, including the addition of the East Bay Express Way and jetty (each 4 meters high), are manually incorporated in the fused DEM, which is particularly crucial for Gwadar. Finally, the terrain roughness is assigned using Manning's Coefficient with values ranging as 0.015 sea floor and open land, 0.03 thinly populated areas, 0.05 moderately populated areas to 0.08 densely populated areas. The coefficient's assignment is based on a fieldwork, photographs, and Google Earth Satellite Images.

3.2.3 Vulnerability analysis

Damage probability refers to the likelihood or probability of damage that a particular type of property will sustain because of tsunami inundation. The inundation analysis (depths-flow velocities and discharge) from numerical modeling of tsunamis, fragility curves can be derived for the areas susceptible to flooding. The vulnerability analysis in our case is carried out by ~~comparing~~ providing our modelling results with the fragility curves for structural damage developed by Koshimura et al. (2009) and Rehman and Cho (2016). These curves are developed for low-rise, lightly reinforced, non-engineered RC (see Fig. 8). The major structure types in Pasni and Gwadar are single-double story structures with conventional masonry and lightly engineered reinforced concrete (RC). The structural and building material types in the Gwadar and Pasni are based on visual estimates carried out during the field work and need to be worked on in detail for better results. The drag force (~~hydrodunamic~~hydrodynamic) per unit width of a structure, expressed mathematically as follows,

$$F = \frac{1}{2} C_D \rho u^2 D$$

where C_D is the drag coefficient equal to 0.99 (1.0 for simplicity), ρ is water density (1,000 kg-m^{-3}), u is the wave velocity (m-s^{-1}), and D the inundation/ flow depth (m). The damage probability for each scenario is calculated using hydrodynamics at the monitoring points (M1 to M7) in both study areas.

4 Results and Interpretations

~~The results of both models are presented city wise and under each heading, the hydrodynamic results are followed by the static modelling results.~~

Pasni scenarios

In the scenario with a 7 m wave, the first wave takes 20 minutes to reach its maximum inundation limit, partly affecting localities such as Wadsar and Main Bazar. The monitoring point M5 experiences a maximum depth of 1 meter and flow velocity of 0.5 m/s. However, areas like Shol, Parhag, and a significant part of the main Pasni town remain relatively unaffected (see Fig. 2A).

In the 10 m wave scenario, a secondary wave with a wave height of 8 m is generated due to reflection from the cliffs northeast of Pasni (Supplements: Simulations-3 Pasni 10 m scenario). These two waveforms reach the Pasni Beach at intervals of 20 minutes and 45 minutes, respectively, following the earthquake (Fig. 3A M6). In both cases, the inundation pattern shifts based on wave direction: northward propagation results in southeast impact, while southward propagation causes inundation from the northeast due to reflection. Initially, the approaching wave inundates the study area from south and inundation extent decreases significantly northward, primarily due to the adjacent river (Shadi Kaur) consuming a significant portion of the inundating wave, resulting in lower water levels in the populated area. Nonetheless, the inundation dynamics pose a significant threat to loss of life and property. The spatial variation of inundation dynamics gradually decreases from south to north, with maximum flow depth, flow velocity at M1 being 6 m - 2.5 ms^{-1}, decreasing to 2 m - 1 ms^{-1} at M6. Also all three scenarios, the maximum flow velocity is recorded through the first wave and maximum flow depth is recorded at quasi-still stand. Quasi-still stand refers to temporary pause or halt at maximum inundation limit after which the backwash process initiates. The backwash tsunami phenomenon persists for more than 4 hours.

~~The Shol and Parhag areas in both models (static and dynamic) remained unaffected by the inundating wave. The Wadsar and north of Main Pasni Town (M6) experience an inundation depth of maximum 3 m and 2 m, respectively, which is somehow close to that of the dynamic model. However, the inundation extents on both sites are underestimated at 400 m and 450 m, respectively, in comparison to the dynamic model. Moreover, the results of Main Bazar and surrounding areas are severely compromised by the static model, where the inundation extent is underestimated by 700 m (see Fig. 3B). These lower estimates keep the Main Bazar uninundated. As already mentioned in the limitations section, the lower estimations are due to the reflection phenomenon, which is not inherited by the static model.~~

In 15 m scenario, the inundation impact is approximately double in terms of flow depth as compared to that in the 10 m scenario due to the heightened wave characteristics and enhanced reflection phenomenon. The approaching and reflecting

Formatted: Subscript

Formatted: Font: (Default) Times New Roman, Font color: Auto, Pattern: Clear

Formatted: Font: (Default) Times New Roman, Font color: Auto, Pattern: Clear

Formatted: Font: (Default) Times New Roman, Font color: Auto, Pattern: Clear

Formatted: Font: (Default) Times New Roman, Font color: Auto, Pattern: Clear

Formatted: Font: (Default) Times New Roman, Font color: Auto, Pattern: Clear

waves interact for a duration of 30 minutes, generating a series of wavelets that gradually increase in intensity and contributing to the formation of a larger and more complex waveform. Consequently, a significant accumulation of water along the shoreline in the study area results in deeper inundation (Supplements: Simulations-4 Pasni 15 m scenario). The wave spectral characteristics exhibit a higher degree of complexity and variability in comparison to the corresponding flow depth. In the densely populated human areas, such as Pasni, Main Bazar, Parhag, and Wadsar, the primary residential zones, we observe peak flow depths ranging between 6 to 8 meters, alongside maximum flow velocities reaching 1.5 ms^{-1}. The intense backwash process observed in this scenario poses a significant hazard, as evidenced by the consistent recording of flow depths exceeding 1 meter at all monitoring points until the 5-hour simulation duration (Fig).

4.~~1 Pasni 7 m Scenario~~

~~The first wave took 20 minutes from the shore to reach its maximum height, or runup height, at Wadsar and Parhag (Supplements: Simulations-2 Pasni 7 m scenario). The waves have the potential to partly inundate Wadsar town and Main Bazar towns (see Fig. 2A). Further northward, the inundation reaches the main road of Pasni city. The Shol, Parhag, and major portions of the main Pasni town remain unaffected by this scenario. The inundation pattern in the 7 m wave scenario is simple as compared with the 10 m and 15 m scenarios. The reflection phenomenon is also faint and could not generate higher waveforms, due to which the impact of the second wave (4 m) is significantly less. The static and dynamic modelling results best match this scenario (see Fig. 2B). To our assessment and understanding, the reflection and amplification phenomena lose their strength as the wave scenario gets smaller. So, we expect an even better match for further smaller wave scenarios.~~

~~4.2 Pasni 10 m Scenario~~

~~In the 10 m wave scenario, along with the approaching wave a secondary wave is generated due to the reflection from the cliffs NE of the Pasni (Supplements: Simulations-3 Pasni 10 m scenario). These two waveforms approach Pasni Beach in 20 minutes and 45 minutes, respectively, after the earthquake (see Fig. 3A M6). Due to the large wavelength, the reflecting wave edge interacts with the approaching part of the wave, resulting in integration and amplification. The reflection source being in the northeast, the second wave pounds the city from the north. The area south-east of Wadsar (uninhabited) is most vulnerable to the extreme waves, with maximum flow depth and flow velocity of 4 m and 1.6 m/s, respectively, due to its low topography and proximity. Next, the Wadsar and the Main Bazar are the worst-affected areas. A maximum inundation extent of 1.2 km is recorded, reaching approximately the location of Mrs. Tanoko House (see Fig. 1B). On the city centre side, the inundating waves reach up to the huge dunes west of Pasni, sweeping the Main Bazar completely with a flow depth and flow velocity of 3 m and 1.3 m/s, respectively. Further from here, the inundation extent decreases northward. The decrease is significant, although the topography and demography are nearly the same. This is because the adjoining river (Shadi Kaur) consumes a major portion of the inundating wave, leaving behind less water budget to inundate the populated area. However, even with this inundating pattern, the life and property losses are high. The back-wash tsunami phenomenon takes about 4 hours. A 10 m high wave (λ/2= 25km) is in closest agreement with the field observations of the 1945 tsunami.~~

~~The Shol and Parhag areas in both models (static and dynamic) remained unaffected by the inundating wave. The Wadsar and north of Main Pasni Town (M6) experience an inundation depth of maximum 3 m and 2 m, respectively, which is somehow close to that of the dynamic model. However, the inundation extents on both sites are underestimated at 400 m and 450 m, respectively, in comparison to the dynamic model. Moreover, the results of Main Bazar and surrounding areas are severely compromised by the static model, where the inundation extent is underestimated by 700 m (see Fig. 3B). These lower estimates keep the Main Bazar uninundated. As already~~

Formatted: Heading 2

Formatted: Heading 2

~~**mentioned in the limitations section, the lower estimations are due to the reflection phenomenon, which is not inherited by the static model.**~~

~~**4.3 Pasni 15 m Scenario**~~

~~In this scenario, a huge pile of water results from reflection, integration, and amplification which inundates deep into the Pasni and surrounding areas (Supplements: Simulations 4 Pasni 15 m scenario). The refection phenomenon has extremely devastating consequences as two gigantic reflecting waves completely drown the whole populated land. The whole Pasni, Wadsar and Parhag experiences a flow depth of 6-8 m, except Shol, where it is 3 m (see Fig. 4A). The inundation impact in terms of flow depth and extents doubles as compared to that in 10 m scenario, especially the later with flow depths of 7 m at the Wadsar monitoring point (M3). Based on the above observations, it is interpreted that the number of waves and the time delay at Pasni have a relationship with the wavelength of the approaching wave. The time delay proxy may be used for the inverse calculations to estimate waveforms during the 1945 tsunami, but the information on the time delay of the 1945 Tsunami is not adequate to perform the test. The depth-average flow velocities show anomalous observations, as near the Pasni (M2), the peak value observed is only 2 m/s against a flow depth of 8 m. We interpreted this as due to the energy loss caused by the reflection, integration, and amplification phenomena.~~

~~The static model severely underestimated the results as compared to those of the dynamic model. The static model could not inundate the Shol, Parhag, and half of the main Pasni town; however, these areas experienced 3 m, 6 m, and 8 m flow depths in dynamic modelling (see Fig. 4B). The reason is the same as discussed before (reflection and integration of waves), and in this scenario, the phenomenon is further amplified. Amplification exposes the coast to large volumes of water as compared to a static or single-wave impact.~~

Gwadar scenarios

The East Gwadar Bay or simply the east bay is characterized by two prominent coastal wave reflectors; one to the north as coastal mountains namely Mehdi-Koh and other to the south as Gwadar Hammer Head (FIG). The Gwadar Hammer Head is a geological formation characterized by a protruding landmass extending into the sea. The subsequent reflection phenomena and the ingress of regular tsunami waves (≤ 4m) contribute to wave integration and amplification along with delayed wave arrivals. For instance, in the 7 m scenario, at M1 (Mohalla Band locality), the first wave arrives 30 minutes after the earthquake, with a flow depth of 1 m. Further, with a lapse of 15 minutes, the second wave inundates the area and increases the flow depth to 2.6 m. This is succeeded by a third wave after a lapse of an additional 30 minutes further increasing the flow depth to 3 m. After the third and final wave the quasi still stand or a temporary stabilization in water prevails for 15 minutes. Hence, with the reflection mechanism in place, the water level exhibits a continuous increase over a span of 60 minutes. However, if we eliminate the influence of reflection from the first tsunami wave, this duration would be reduced to merely 15 minutes with only 1 m flow depth at M1. The wave spectral analysis shows an inverse relation of flow depth and flow velocity because of the loss of kinetic energy during reflection-amplification phenomenon.

The Surbandar locality (M4) remains unaffected in the 7 m scenario, however in 10 m and 15 m scenarios the locality is severely affected. The Surbandar locality, positioned at a lower elevation compared to the beach banks in the south from the tsunami propagates, experiences wave overflow during tsunamis. Being situated on low-lying topography as compared to the beach banks and by the direct facing to the tsunami, the torrential force achieves a flow velocity of 4 ms^{-1} and 6 ms^{-1} in 10 m scenario and 15 m scenario, respectively. Similar phenomenon is observed for Pishukan locality (M5). The cliffs, averaging a height of 12 meters, situated to the south of Pishkun provide protection against inundation in scenarios of 7 m and 10 m. However, in the 15 m scenario, waves spill over these defenses, resulting in observed flow depths and velocities of 3 m and 2.1 ms-1 respectively at M5. The New Town locality (M2) exhibits the highest flow depth in each scenario, reflecting its heightened vulnerability to tsunami inundation. Analysis reveals that this high vulnerability arises from inundation originating from both the east and west bays, where wave interactions lead to amplification of the inundating waves.

In the Gwadar town (M1 to M2), both sides of the bay are elevated to a height of 5 meters above mean sea level (MSL) to accommodate road construction. This elevated terrain, coupled with an inadequate and low-capacity drainage infrastructure, significantly impedes the backwash process of tsunamis (see Figure). Modeling results indicate a flow depth exceeding 2 m in the Gwadar town even after three hours."

~~**4.4 Gwadar 7 m Scenario**~~

~~The 7 m wave scenario affects Gwadar and Surbandar; however, the Pishukan remains unaffected. At Gwadar, the waves inundate both bays; on the eastern bay, Mohalla and the adjoining seaport are affected with flow depth and flow velocity of 3 m and 1.6 m/s, respectively (see Fig. 5A M1). This is the same area that underwent severe damage in the 1945 tsunami (Kakar et al., 2014). The morphology of Gwadar city has changed much from what it was in 1945 due to the construction of raised road highways that are averagely 4 m (from the high tide line) high on both sides of the bay bordering the city. These bordering structures act as defence structures against tsunamis and storm related waves. The 1945 tsunami height at Gwadar was not exactly recorded or reported. According to our analysis based on the survivor's interviews and dynamic modelling results, the tsunami wave height was around 6 m to 7m. Only the eastern side facing the tsunami source was affected. As the inundation dynamics change with source location and we projected the waves from the whole MSZ, the inundation occurs at the New Town also by flow depth and flow velocity of 3.6 m and 1.3 m/s, respectively.~~

~~The defence structures temporarily dammed the city, due to which the backwash phenomenon took a considerably large amount of time. Also, a poor and low-capacity drainage network further retards the process. The Mohalla, spread over a 4.5 km2 area, remained under water at a depth of 2 m even after 4 hours (see Fig. 5A M1). At New Town (~4 km2), backwash further aggravates, with a water depth of 2.5 m for the complete period of simulation (see Fig. 5A M2).~~

Reflection, integration, and amplification are common devastating phenomena observed in Pasni and Gwadar. In the case of the 7 m scenario, three reflective waves are generated in addition to the approaching wave (see Fig. 5A M1). Of these three, two are 7 m high and one <0.4 m high. The reflective waves, while propagating southward, strike the Gwadar-Hammer-Head structure (highlands) and find their way to the Mohalla Band area (Supplements: Simulations-6 Gwadar 7 m scenario). Each wave exacerbates the effect of inundation. This effect is conspicuous at Mohalla Band monitoring point (M1), where the flow depths and flow velocities increase gradually from 1 m and 0.5 m/s (wave-1) to 3 m and 1.0 m/s (wave-3). More or less similar inundation dynamics occur at the New Town locality on the western Gwadar Bay. The proposed future industrial site is also vulnerable to this wave scenario. The Surbandar locality narrowly escaped the tsunami inundation. Though the waves overtop or overflow the beachbanks, following the low-lying topography, the tsunami torrent bypasses the populated area and drains back into the sea. The Pishukan, due to its high topography, stays safe in this scenario. The boats at the docking site or related installments may suffer minor damage.

The static model results are only comparable to those of the first dynamic wave (see Fig. 5B); however, the simulation shows that the worst comes with reflection and amplification phenomena. For this reason, the static model overestimates the beach proximity and underestimates the inundation extents.

4.5 Gwadar 10 m Scenario

The inundation pattern of the 15 m scenario is almost identical to that of the 7 m scenario, but the inundating dynamics (flow, depth, and extent) are more than twice as large as those in the 7 m scenario. Almost complete Gwadar-Hammer-Head-Neck (Gwadar city) and Surbandar experience inundation, and Pishukan remains un-inundated again (see Fig. 6A). The Mohalla Band and New Town receive three waves, which gradually increase the flow depth from 3 m to 5 m and 5 m to 7 m, respectively. At the New Town, the approaching-reflective wave interval is very short, due to which both wave forms superimpose over one another and make a plateau-shaped flow depth graph. The inundating extents from both sides of the Gwadar Bays overlap to completely submerge the town (Supplements: Simulations-7 Gwadar 10 m scenario). A maximum inundation extent of 4.5 km is observed across the industrial area (M3), facilitated by a stream in its northern vicinity. It is observed that maximum flow velocity is experienced when a site is directly facing the approaching wave. Also, much of the wave energy is lost during the reflection phenomenon. These two observations are based on a comparative analysis of flow velocities between approaching and reflecting waves. For instance, at the Mohalla Band, an approaching wave has a maximum flow depth of 3 m and a flow velocity of 2 m/s. Further, the two reflected waves increase the flow depths to 5 m, but flow velocities decrease to <0.5 m/s. The lateral two piled up huge amounts of water at the coast, but energy (velocity) decreased around threefold. Surbandar is the only locality that directly faces the approaching wave and experiences the highest flow velocity of 4 m/s with a flow depth of 6 m. The static model did not produce adequate and satisfactory results in this scenario. It overestimates the flow depths approximately by a factor 2 at the beach proximity and underestimates the inundation extents as it lacks parameters to estimate the reflection input (see Fig. 6B).

~~**4.6 Gwadar 15 m Scenario**~~

~~In the 15 m wave scenario, the reflection and amplification phenomena further gain momentum. For instance, the peak flow depth at Mohalla Band (M1) in a 10 m scenario and a 15 m scenario is 5 m and 12 m, respectively. Here, the flow depth in the latter case is increased by a factor of 2 in relation to the approaching wave height and wavelength. Also, with a higher wave scenario, the time interval between the reflecting waves decreases, resulting in a quick overlap of major wave portions, and only small wave crests are observed in the flow depth graph trajectories. At the Mohallah Band, New Town, Industrial, and Surbandar localities, the immense inundation takes place for about 25 minutes and then starts the backwash (see Fig. 7A). As already discussed, these two localities are embanked by the raised road highways. The entrapped or dammed water only finds its way through the sewerage or drainage network. This is why the first two localities remain more than 2 m under water even after hours in all scenarios. The Gwadar-Hammer-Head receives a weekly wave reflection after four hours, which has minor effects on the flow depths and flow velocities (see Fig. 7A). In a 15 m scenario that inundates the whole Surbandar, the maximum flow depth is 11 m with a very high flow velocity of 6 m/s. In this scenario, the flow depth doubles as compared to the 10 m wave scenario. The scenario will be terrible as an approaching wave overtops the beach cliffs; the northward downstream rushing water will completely scrape off the town (Supplements: Simulations 8 Gwadar 15 m scenario).~~

~~As it overtopped the ridge, the Surbandar community may not visually notice the approaching wave before impact, due to which the earlier unwarned community only has less than a minute to climb up the higher grounds. Consequently, the casualty rate may be much higher here. The Pishukan town could not evade this scenario and receive overtopped waves from the southern beach cliffs as well as those of Surbandar. It experiences a maximum flow depth and wave velocity of 3 m and 2 m/s, respectively. With the approaching wave visually hidden behind the cliffs as in Surbandar, the earlier unwarned community has a maximum of 4 minutes to find the safe sites. Due to the high impact of reflection, integration, and amplification processes, we did not carry out the comparative analysis between static and dynamic modelling. However, the static model highly underestimates the scenario (see Fig. 7B).~~

5. Vulnerability Analysis

The damage probability for each scenario is assessed through hydrodynamic analysis conducted at monitoring each point in both cities. Consequently, damage intensity is expected to escalate towards the shoreline from these monitoring locations. However, exceptions are noted in the cases of Surbandar and Pishukan in Gwadar, which are elaborated later.

At Pasni, monitoring points M1 and M2 exhibit the most severe flow dynamics, indicating the highest vulnerability to tsunami inundation in each scenario. For M1, the damage probabilities are 0.50, 0.95, and 1.0 for the 7 m, 10 m, and 15 m scenarios, respectively. Similarly, for M2, the corresponding probabilities are 0.05, 0.6, and 0.95. Despite being uninhabited, any development should undergo feasibility studies concerning extreme wave events, particularly tsunamis. Regarding the inhabited part, the 7 m scenario minorly affects the Main Bazar locality (M5) and surrounding areas with an estimated

damage probability close to zero. However, it should be noted that infrastructure or communities residing in close proximity to the shoreline may still possess some degree of damage potential. In the 10 m scenario, the Wadsar locality (M3) poses the maximum damage potential with probability of 0.57, followed by Main Bazar (M5) with 0.37, and then Pasni locality (M6) with 0.05. In the 15 m scenario, no locality remains unaffected; all localities exhibit a probability of damage exceeding 0.6, except for Shol (M7), which registers a value of 0.4.

The results indicate that the level of vulnerability and probability of damage are higher in the Gwadar area compared to the Pasni area. In the 7 m scenario, three localities, two of which are inhabited, are inundated. The Mohalla Band locality (M1) exhibits a damage probability of 0.4, followed by the New Town locality (M2) with 0.1. Additionally, the proposed site for industrial development (undeveloped) is also inundated, with a damage probability of less than 0.1.

The 10 m and 15 m scenarios pose significant challenges for the area. In the 10 m scenario, only Pishukan remains unimpacted, while all other localities are anticipated to experience a damage probability exceeding 0.8. The findings indicate that the Surbandar locality (M4) encounters a hydrodynamic force exceeding 40 kNm. This heightened level is attributed to tsunami overtopping the beach banks followed by a torrential downslope runoff effect, as discussed earlier in the section (section). All localities, except Pishukan, have a damage probability of 1.0, with hydrodynamic force exceeding 35 kNm. The Pishukan locality (M5) indicates a probability of 0.6.

6. Discussion and Conclusions

The process of tsunami modeling comprises three distinct phases: generation, propagation, and inundation. The generation phase involves calculation of sea floor deformation during an earthquake causing initial disturbance in the oceanic water. Subsequently, a hydrodynamic model utilizes this initial wave to model and simulate the propagation and inundation of the tsunami waves. For tsunami generation and potential estimation, utilizing Okada's (1985) model for the initial sea floor deformation is a valuable asset in seismic and tsunami hazard assessment. However, it is imperative to refer to the model's inherent limitations and their potential impact on our findings. Primarily, the model's static nature and its reliance on a single linear fault plane geometry, coupled with its exclusion of material properties considerations, pose notable constraints. These constraints may result in an underestimation or overestimation of tsunami hazard levels, emphasizing the need for caution and further investigation when interpreting our results. To have better results for generation and potential estimation, we compiled and analyzed the tsunamites discovered along the Arabian Sea shorelines and took the case exhibiting worse morphodynamics for modeling purposes. Subsequently, utilizing Okada's (1985) fault parameters, various tsunami wave scenarios are generated along the MSZ to find the capable one aligning with both field and laboratory readings of tsunamites

case taken up. As a result, our study provides a better waves tsunami potential estimation and an indirect approximation of potential fault parameters and earthquake potential, offering valuable insights into tsunami hazard assessment.

In tsunami hazard assessment, wave height is considered a yardstick, while wavelength tends to be overlooked. We assessed that for vulnerability and risk assessment, along with wave height, the wavelength must be taken into consideration. To illustrate this point, we conducted simulations involving two scenarios with identical wave heights of 5 m but differing wavelengths ($\lambda/2$) of 15 km and 3 km, impacting the Pasni coast (see Supplements: Simulations-9). The wave with the shorter wavelength dissipated faster without causing any inundation, whereas the longer wavelength resulted in considerable inundation, with a runup height of 2 m and an inundation extent of 0.7 km. This disparity can be attributed to the shorter wavelength, which leads to a smaller quantity of displaced water that disperses rapidly and diminishes in magnitude during propagation, confining the hazards to local areas. Vertical seafloor deformation or coseismic displacement tends to result in tsunamis characterized by longer wavelengths and longer periods when compared to those generated by landslide failures, mainly because of the broader source area associated with coseismic displacement events (Hammack, 1973; Watts, 1998).

The bare ground elevation model represents a digital topography with no building infrastructure, plants, poles, etc. It is formally known as the digital terrain model (DTM). For inundation analysis, the deflection of DEM from DTM hampers the results in two aspects: i) the porous infrastructure, such as houses, mangroves etc., does not account for water balance adjustments. These structures act as solid blocks, occupying the volume and deflecting the inundating water further ahead, resulting in higher inundation extents. ii) In the case of a low-resolution DEM that cannot resolve the streets or passages results in water damming. The damming results in higher flow depths downstream than actual, and it also affects the backwash computations. The results can be improved further by improving the surface roughness values both qualitatively and quantitatively, topographic resolution, and decreasing the computational grid size.

The effectiveness of the tsunami early warning system is assessed in terms of far-field and near-field sources particularly for the study area. An integrated Indian Ocean Tsunami Early Warning System is developed under the framework of Intergovernmental Oceanographic Commission (IOC-IOTWS) under the UNESCO umbrella in response to the tragic tsunami on 26th December 2004. The near-field tsunami warning is issued based on the location, size and initial evaluation of earthquake fault parameters through seismic spectral signatures. The Pakistan Meteorological Department (PMD) in collaboration with IOC-IOTWS is responsible for keeping track of coastal hazards and issuance of tsunami notifications and alerts. Therefore, due to extremely small-time window, for earthquakes Mw $\geq$ 6.5, a near-shore early warning system puts the coastal community immediately under alert and watch status until confirmation of tsunami generation. The tsunami confirmation warning is issued once the tsunami wave is detected on any sensor or tide gauge which is either installed at the coast or DART station (Deep-ocean Assessment and Reporting of Tsunamis). In the study areas these gauges are installed at Gwadar and Pasni ports and the nearest DART station 450 km from the MSZ. The numerical models show, the first tsunami wave generated at eastern MSZ arrives at the Pasni Coast (Pasni tide gauge) and the nearest DART in 15 and 45 minutes, respectively. Heidarzadeh et al. (2007) calculated these timings as 15 and 60 minutes, respectively. If the tsunami had generated at eastern MSZ, it would reach the Makran Coast before its instrumental detection and confirmation warning. So,

the coastal community will surpass the confirmation warning and had to rely on the advisory (alert and watch) warning only. On the other hand, the confirmation warning system works very well for the far-source tsunamis as a number of gauges installed at eastern Indian Coast, Maldives and DART stations detects the propagating tsunami several hours before reaching the Makran Coast (Srinivasa Kumar and Manneela, 2021). Further, three case studies from the Indian Ocean are presented for assessment of general practices and timelines in terms of detection, warning, and confirmation. The timeline for these chain of events during each tsunami case is given in (Table S2 supplements).

Since the installation of IOTWS, 2013 Tsunami is the only near-field tsunami generated in the Arabian Sea. It was triggered remotely by a terrestrial earthquake located near the Khuzdar city, Pakistan. The tsunami waves remained almost unnoticed by the community due to the low wave heights and its occurrence at low tide. As it is thought to be triggered by an underwater landslide, the exact trigger time and location are not known. However, through reverse modelling the source position at offshore of the Pakistan estimated in between Gwadar and MSZ (Hoffmann et al., 2014). Form this tsunami source, the waves would have reached the Gwadar Coast within 5-20 minutes. After the earthquake, the first advisory warning followed by second confirming "no tsunami" warning was issued 11 minutes and 16 minutes, respectively after the earthquake. The advisory warning confirmation was particularly issued on the bases of epicentre being on the terrestrial (inland) part. The tsunami was first detected instrumentally 39 minutes after the earthquake at the Qurayat tide gauge in Oman. Various other tide gauges also recorded the tsunami afterward. The DART detected the tsunami wave 72 minutes after the earthquake. No further warning was issued may be due to small scale of the tsunami. Regarding the far-field tsunami, we analysed two cases: July 17, 2006, Java and October 25, 2010, Mentawai, Indonesia Tsunamis. In both cases, the system worked very well to warn the far-field communities. However, in both cases the waves arrived at nearest coast of Indonesia before issuance of 1st warning (details in Table S2 supplements). The tsunami confirmation warnings in both cases were issued 19 minutes after of the earthquake at international early warning system where all local and regional warning systems are connected. These tsunamis took around 8 hours to reach the Makran Coast providing enough time to inform and evacuate the community. Here, we emphasize the importance of alert-watch awareness and preparedness for the communities residing close to tsunami source. The most common natural tsunami signs are considered as the receding water after an earthquake and a strong and unusual roar sound. The awareness coupled with trainings, route evacuation and to react during such disasters is also very important. The PMD also has a well-established cyclone early warning system operating since 1960s. Despite multiple early warnings issued to coastal communities (couple of days earlier) the high number of fatalities and property losses from the cyclones in 1998, 1999, 2007, 2010, and 2021 demonstrate dismal levels in terms of resilience and preparedness. Likewise, the impact of a tsunami appears to be far harsher.

References

Banghar, A. and Syke, L. R.: Focal mechanism of an earthquake from the Southern Ocean, Tectonophysics, 79, 37–41, 1981.

Behrens, J., Løvholt, F., Jalayer, F., Lorito, S., Salgado-Gálvez, M. A., Sørensen, M., Abadie, S., Aguirre-Ayerbe, I., Aniel-Quiroga, I., Babeyko, A., Baiguera, M., Basili, R., Belliazzi, S., Grezio, A., Johnson, K., Murphy, S., Paris, R., Rafliana, I., De Risi, R., Rossetto, T., Selva, J., Taroni, M., Del Zoppo, M., Armigliato, A., Bureš, V., Cech, P., Cecioni, C., Christodoulides, P., Davies, G., Dias, F., Bayraktar, H. B., González, M., Gritsevich, M., Guillas, S., Harbitz, C. B., Kânoğlu, U., Macías, J., Papadopoulos, G. A., Polet, J., Romano, F., Salamon, A., Scala, A., Stepinac, M., Tappin, D. R., Thio, H. K., Tonini, R., Triantafyllou, I., Ulrich, T., Varini, E., Volpe, M. and Vyhmeister, E.: Probabilistic Tsunami Hazard and Risk Analysis: A Review of Research Gaps, Front. Earth Sci., 9(April), 1–28, doi:10.3389/feart.2021.628772, 2021.

Brune, J. N.: Seismic moment, seismicity, and rate of slip along Major fault zones, J. Geophys. Res., 73(2), 1968.

Byrne, D. E., Sykes, L. R. and Davis, D. M.: Great thrust earthquakes and aseismic slip along the plate boundary of the Makran Subduction Zone, J. Geophys. Res., 97(B1), 449–478 [online] Available from: http://onlinelibrary.wiley.com/doi/10.1029/91JB02165/full, 1992.

Carrier, G. F., WU, T. ailtei and Yeh, H.: Tsunami run-up and draw-down on a plane beach, J. Fluid Mech., 475, 79–99, doi:DOI: 10.1017/S0022112002002653, 2003.

Chacón-Barrantes, S., Narayanan, R. R. A. and Mayerle, R.: Several tsunami scenarios at the North Sea and their consequences at the German Bight., 2013.

Deltares: Delft3d-Flow; simulation of multi-dimensional hydrodynamic flows and transport phenomena, including sediments. https://content.oss.deltares.nl/delft3d4/Delft3D-FLOW_User_Manual.pdf, , 1–725, 2017.

El-Hussain, I., Omira, R., Deif, A., Al-Habsi, Z., Al-Rawas, G., Mohamad, A., Al-Jabri, K. and Baptista, M. A.: Probabilistic tsunami hazard assessment along Oman coast from submarine earthquakes in the Makran subduction zone, Arab. J. Geosci., 9(15), doi:10.1007/s12517-016-2687-0, 2016.

Gates, G. O., Page, W. D., Savage, W. U. and Zuberi, S.: The Makran Earthquake November 28, (Mag. 8.3)1975 Field appraisal of geology and cultural effects, in The Sixth World Conference on Earthquake Engineering New Delhi, India., 1977.

Gelfenbaum, G., Vatvani, D., Jaffe, B. and Dekker, F.: Tsunami inundation and sediment transport in vicinity of coastal mangrove forest, Coast. Sediments '07 - Proc. 6th Int. Symp. Coast. Eng. Sci. Coast. Sediment Process., 1–12, doi:10.1061/40926(239)86, 2007.

Haider, R., Ali, S., Hoffmann, G. and Reicherter, K.: A multi-proxy approach to assess tsunami hazard with a preliminary risk assessment: A case study of the Makran Coast, Pakistan, Mar. Geol., 107032, doi:https://doi.org/10.1016/j.margeo.2023.107032, 2023.

Hammack, J. L.: A note on tsunamis: Their generation and propagation in an ocean of uniform depth, J. Fluid Mech., 60(4), 769–799, doi:10.1017/S0022112073000479, 1973.

Hanks, T. C. and Kanamori, H.: A moment magnitude scale, J. Geophys. Res. B Solid Earth, 84(B5), 2348–2350, doi:10.1029/JB084iB05p02348, 1979.

Harbitz, C. B., Løvholt, F. and Bungum, H.: Submarine landslide tsunamis: How extreme and how likely?, Nat. Hazards, 72(3), 1341–1374, doi:10.1007/s11069-013-0681-3, 2014.

Heidarzadeh, M. and Satake, K.: New Insights into the Source of the Makran Tsunami of 27 November 1945 from Tsunami Waveforms and Coastal Deformation Data, Pure Appl. Geophys., 172(3–4), 621–640, doi:10.1007/s00024-014-0948-y, 2014a.

Heidarzadeh, M. and Satake, K.: Possible sources of the tsunami observed in the northwestern Indian ocean following the 2013 September 24 Mw 7.7 Pakistan inland earthquake, Geophys. J. Int., 199(2), 752–766, doi:10.1093/gji/ggu297, 2014b.

Heidarzadeh, M., Pirooz, M. D., Zaker, N. H. and Mokhtari, M.: Modeling of tsunami propagation in the vicinity of the southern coasts of Iran, Int. J. Civ. Eng., 5(4), 223–234, doi:10.1115/OMAE2007-29082, 2007.

Heidarzadeh, M., Pirooz, M. D., Zaker, N. H., Yalciner, A. C., Mokhtari, M. and Esmaeily, A.: Historical tsunami in the Makran Subduction Zone off the southern coasts of Iran and Pakistan and results of numerical modeling, Ocean Eng., 35(8–9), 774–786, doi:10.1016/j.oceaneng.2008.01.017, 2008.

Heidarzadeh, M., Pirooz, M. D., Zaker, N. H. and Yalciner, A. C.: Preliminary estimation of the tsunami hazards associated with the Makran subduction zone at the northwestern Indian Ocean, Nat. Hazards, 48(2), 229–243, doi:10.1007/s11069-008-9259-x, 2009.

Hoffmann, G., Reicherter, K., Wiatr, T., Grützner, C. and Rausch, T.: Block and boulder accumulations along the coastline between Fins and Sur (Sultanate of Oman): Tsunamigenic remains?, Nat. Hazards, 65(1), 851–873, doi:10.1007/s11069-012-0399-7, 2013a.

Hoffmann, G., Rupprechter, M., Balushi, N. Al, Grützner, C. and Reicherter, K.: The impact of the 1945 Makran tsunami along the coastlines of the Arabian Sea (Northern Indian Ocean) – a review, Zeitschrift für Geomorphol. Suppl. Issues, 57(4), 257–277, doi:10.1127/0372-8854/2013/s-00134, 2013b.

Hoffmann, G., Al-Yahyai, S., Naeem, G., Kociok, M. and Grützner, C.: An Indian Ocean tsunami triggered remotely by an onshore earthquake in Balochistan, Pakistan, Geology, 42(10), 883–886, doi:10.1130/G35756.1, 2014.

Hoffmann, G., Grützner, C., Schneider, B., Preusser, F. and Reicherter, K.: Large Holocene tsunamis in the northern Arabian Sea, Mar. Geol., 419(September 2019), doi:10.1016/j.margeo.2019.106068, 2020.

Jade, S., Shrungeshwara, T. S., Kumar, K., Choudhury, P., Dumka, R. K. and Bhu, H.: India plate angular velocity and contemporary deformation rates from continuous GPS measurements from 1996 to 2015, Sci. Rep., 7(1), 1–16, doi:10.1038/s41598-017-11697-w, 2017.

Jaiswal, R. K., Singh, A. P. and Rastogi, B. K.: Simulation of the Arabian Sea Tsunami propagation generated due to 1945 Makran Earthquake and its effect on western parts of Gujarat (India), Nat. Hazards, 48(2), 245–258, doi:10.1007/s11069-008-9261-3, 2009.

Kakar, D. M., Naeem, G., Usman, A., Hasan, H., Lohdi, H. A., Srinivasalu, S., Andrade, V., Rajendran, C. P., Beni, A. N.,

Hamzeh, M. A. and Hoffmann, G.: Elders recall an earlier tsunami on Indian Ocean shores, Eos, Trans. Am. Geophys. Union, 95(51), 485–486 [online] Available from: https://www.iotic.ioc-unesco.org/, 2014.

Khaledzadeh, M. and Ghods, A.: Estimation of size of megathrust zone in the Makran subduction system by thermal modelling, Geophys. J. Int., 228(3), 1530–1540, doi:10.1093/gji/ggab417, 2022.

Khan, M. A., Bendick, R., Bhat, M. I., Bilham, R., Kakar, D. M., Khan, S. F., Lodi, S. H., Qazi, M. S., Singh, B., Szeliga, W. and Wahab, A.: Preliminary geodetic constraints on plate boundary deformation on the western edge of the Indian plate from TriGGnet (Tri-University GPS Geodesy Network), J. Himal. Earth Sci., 41(May), 71–87, 2008.

Koshimura, S., Oie, T., Yanagisawa, H. and Imamura, F.: Developing fragility functions for tsunami damage estimation using numerical model and post-tsunami data from banda aceh, Indonesia, Coast. Eng. J., 51(3), 243–273, doi:10.1142/S0578563409002004, 2009.

Koster, B., Hoffmann, G., Grützner, C. and Reicherter, K.: Ground penetrating radar facies of inferred tsunami deposits on the shores of the Arabian Sea (Northern Indian Ocean), Mar. Geol., 351, 13–24, doi:10.1016/j.margeo.2014.03.002, 2014.

Kukowski, N., Schillhorn, T., Flueh, E. R. and Huhn, K.: Newly identified strike-slip plate boundary in the northeastern Arabian Sea, Geology, 28(4), 355–358, doi:10.1130/0091-7613(2000)28<355:NISPBI>2.0.CO;2, 2000.

Løvholt, F.: Tsunami Hazard and Risk Assessment, United Nations Off. Disaster Risk Reduct., (July), 1–9 [online] Available from: https://www.unisdr.org/we/inform/publications/57441, 2017.

Macintosh, A.: Coastal climate hazards and urban planning : how planning responses can lead to maladaptation, , 1035–1055, doi:10.1007/s11027-012-9406-2, 2013.

Madsen, P. er A. and Schaeffer, H. A.: Analytical solutions for tsunami runup on a plane beach: single waves, N-waves and transient waves, J. Fluid Mech., 645, 27–57, doi:DOI: 10.1017/S0022112009992485, 2010.

Neetu, S., Suresh, I., Shankar, R., Nagarajan, B., Sharma, R., Shenoi, S. S. C., Unnikrishnan, A. S. and Sundar, D.: Trapped waves of the 27 November 1945 Makran tsunami: Observations and numerical modeling, Nat. Hazards, 59(3), 1609–1618, doi:10.1007/s11069-011-9854-0, 2011.

Okada, Y.: Surface deformation due to shear and tensile faults in a half space, Bull. - Seismol. Soc. Am., 75(4), 1135–1154, doi:10.1785/bssa0820021018, 1985.

Van Ormondt, M., Nederhoff, K. and Van Dongeren, A.: Delft Dashboard: A quick set-up tool for hydrodynamic models, J. Hydroinformatics, 22(3), 510–527, doi:10.2166/hydro.2020.092, 2020.

Page, W. D., Alt, J. N., Cluff, L. S. and Plafker, G.: Evidence for the recurrence of large-magnitude earthquakes along the makran coast of Iran and Pakistan, Tectonophysics, 52, 533–547, doi:10.1016/B978-0-444-41783-1.50081-7, 1979.

Park, S., van de Lindt, J. W., Cox, D. and Gupta, R.: Concept of Community Fragilities for Tsunami Coastal Inundation Studies, Nat. Hazards Rev., 14(4), 220–228, doi:10.1061/(asce)nh.1527-6996.0000092, 2013.

Pendse, C. G.: The Mekran Earthquake of the 28th November 1945, Sci. Notes, X(125), 141–146, 1946.

Rehman, K. and Cho, Y. S.: Building damage assessment using scenario based tsunami numerical analysis and fragility curves, Water (Switzerland), 8(3), doi:10.3390/w8030109, 2016.

Reilinger, R., McClusky, S., Vernant, P., Lawrence, S., Ergintav, S., Cakmak, R., Ozener, H., Kadirov, F., Guliev, I., Stepanyan, R., Nadariya, M., Hahubia, G., Mahmoud, S., Sakr, K., ArRajehi, A., Paradissis, D., Al-Aydrus, A., Prilepin, M., Guseva, T., Evren, E., Dmitrotsa, A., Filikov, S. V., Gomez, F., Al-Ghazzi, R. and Karam, G.: GPS constraints on continental deformation in the Africa-Arabia-Eurasia continental collision zone and implications for the dynamics of plate interactions, J. Geophys. Res. Solid Earth, 111(5), 1–26, doi:10.1029/2005JB004051, 2006.

Röbke, B. R., Schüttrumpf, H. and Vött, A.: Effects of different boundary conditions and palaeotopographies on the onshore response of tsunamis in a numerical model - A case study from western Greece, Cont. Shelf Res., 124(September 2000), 182–199, doi:10.1016/j.csr.2016.04.010, 2016.

Röbke, B. R., Schüttrumpf, H. and Vött, A.: Hydro- and morphodynamic tsunami simulations for the ambrakian gulf (Greece) and comparison with geoscientific field traces, Geophys. J. Int., 213(1), 317–339, doi:10.1093/gji/ggx553, 2018.

Rodriguez, M., Fournier, M., Chamot-Rooke, N., Huchon, P., Bourget, J., Sorbier, M., Zaragosi, S. and Rabaute, A.: Neotectonics of the Owen Fracture Zone (NW Indian Ocean): Structural evolution of an oceanic strike-slip plate boundary, Geochemistry, Geophys. Geosystems, 12(12), doi:10.1029/2011GC003731, 2011.

Smith, G. L., McNeill, L., Henstock, I. J. and Bull, J.: The structure and fault activity of the Makran accretionary prism, J. Geophys. Res., 117(7), 1–17, doi:10.1029/2012JB009312, 2012.

Srinivasa Kumar, T. and Manneela, S.: A Review of the Progress, Challenges and Future Trends in Tsunami Early Warning Systems, J. Geol. Soc. India, 97(12), 1533–1544, doi:10.1007/s12594-021-1910-0, 2021.

Sujatmiko, K. A., Ichii, K., Murata, S. and Mulia, I. E.: Application of Stress Parameter from Liquefaction Analysis on the Landslide Induced Tsunami Simulation : A Case Study of the 2018 Palu Tsunami, , 18(3), 199–208, doi:10.20965/jdr.2023.p0199, 2023.

Tadepalli, S. and Synolakis, C. E.: The run-up of N-waves on sloping beachest, , 445(1923), 99–112, 1994.

Tarbotton, C., Dall'Osso, F., Dominey-Howes, D. and Goff, J.: The use of empirical vulnerability functions to assess the response of buildings to tsunami impact: Comparative review and summary of best practice, Earth-Science Rev., 142, 120–134, doi:https://doi.org/10.1016/j.earscirev.2015.01.002, 2015.

Vernant, P., Nilforoushan, F., Hatzfeld, D., Abbassi, M. R., Vigny, C., Masson, F., Nankali, H., Martinod, J., Ashtiani, A., Bayer, R., Tavakoli, F. and Chéry, J.: Present-day crustal deformation and plate kinematics in the Middle East constrained by GPS measurements in Iran and northern Oman, Geophys. J. Int., 157(1), 381–398, doi:10.1111/j.1365-246X.2004.02222.x, 2004.

Watts, P.: Wavemaker Curves for Tsunamis Generated by Underwater Landslides, J. Waterw. Port, Coastal, Ocean Eng., 124(3), 127–137, doi:10.1061/(asce)0733-950x(1998)124:3(127), 1998.

Zaccagnino, D., Telesca, L. and Doglioni, C.: Scaling properties of seismicity and faulting, Earth Planet. Sci. Lett., 584(March), 117511, doi:10.1016/j.epsl.2022.117511, 2022.

Figures and tables

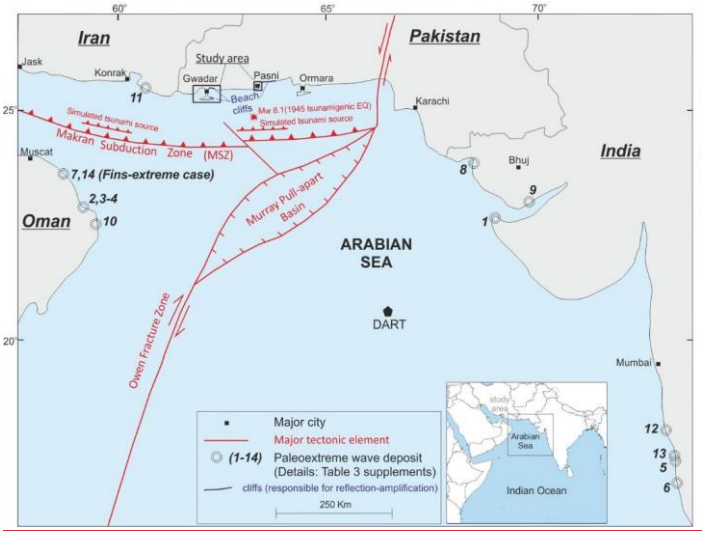

615

Figure 1: A Location and tectonic map of the study areas (Gwadar, Pasni). The circles with numbers show the reported palaeoextreme wave deposits; details are in Table S1 in the supplements. DART: Deep-ocean Assessment and Reporting of Tsunamis.

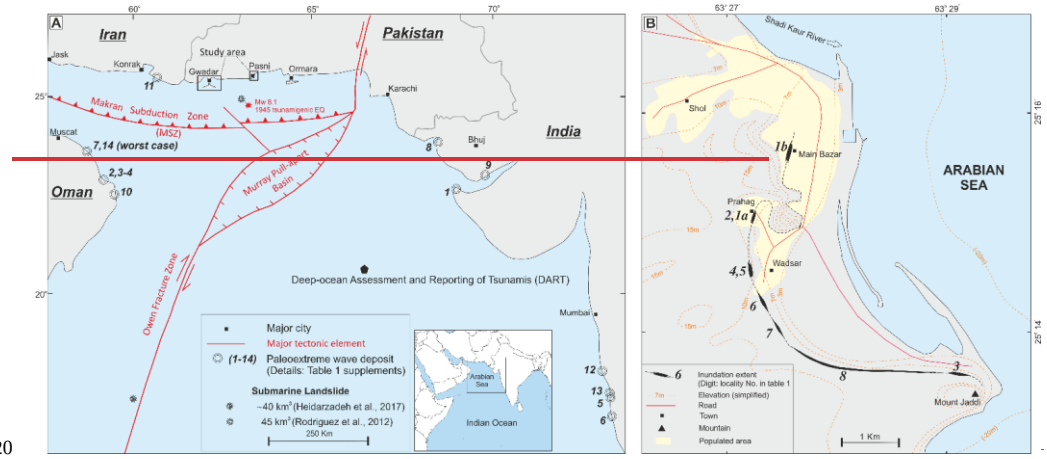

~~Figure 1: A Location and tectonic map of the study area. The circles with numbers show the reported palaeoextreme wave deposits; details are in Table S1 in the supplements. B Map showing inundation extents during the 1945 tsunami in the Pasni area. The mapping is based on the interviews and the field observations given in Table 2.~~Table 1: Table showing the earthquake source parameters used to model each scenario with respective initial wave height.

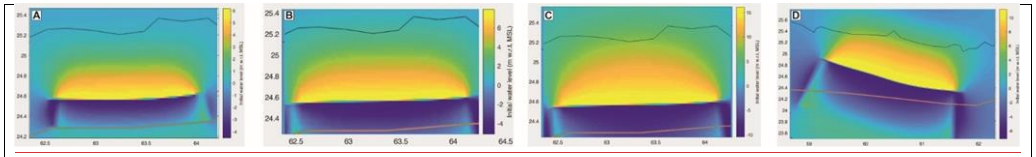

Initial Wave height		Length (km)	Strike (deg)	Width (km)	Depth (km)	Dip (deg)	Rake (deg)	Slip (m)
A	East	200	266 to 269	110	10	35	90	8
B	MSZ	200	266 to 269	160	10	35	90	10
C	(study area)	200	266 to 269	211	10	35	90	22
D (Fins)		200	-84 to -70	211	10	35	90	22

Scenario D represents the initial wave height generated for modeling the Fins Tsunamites case.
Scenarios A, B, and C represent the initial wave heights for the Pasni and Gwadar areas.

Table 2: Summarized methodology with flowchart showing sequential order of various processes used for hazard and vulnerability assessment.

Formatted: Normal

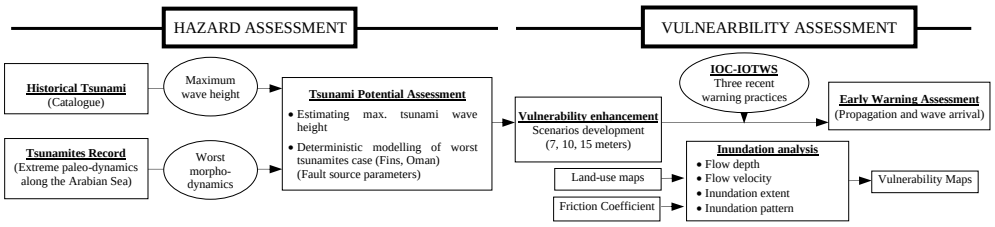

Approach	Model	Equation/s	Reference
Hydrodynamic	**Delft3D (Flow module, Dashboard)** • mass conservation • momentum eq. • surface roughness • simulations	• *Hydrodynamic equations* • *Continuity equation* • *Momentum equations in horizontal direction* • *Vertical velocities* • *Hydrostatic pressure assumption* • *Coriolis force and Reynolds stresses equations* * For details, referred to (Deltares, 2023), pp. 168–186)	(Deltares, 2023) (Gelfenbaum et al., 2007) (Chacón-Barrantes et al., 2013) (Röbke et al., 2016) (Röbke et al., 2018) (Van Ormondt et al., 2020) (Sujatmiko et al., 2023)

Formatted: Normal

~~**Table 2: Table showing the compilation of inundation facts at Pasni from the interviews of 1945 survivors and the field observations.**~~

~~Interviewee~~	~~Age (years as of 1945)~~	~~Brief description~~	~~Run-up height~~	~~Inund. extent~~	~~Locality No. in Figure 1B~~
~~Tanakko Bibi~~	~~11~~	~~a) "The 1945 tsunami came up until here, where we are sitting right now (her house). You can still see the seashells (of the 1945 tsunami) scattered around here.""~~ ~~b) "Much of the casualties happened in the Main Bazar locality"~~	~~9 m~~ ~~7 m~~	~~1.6 km~~ ~~1.3 km~~	~~1a~~ ~~1b~~
~~Rabia Bibi*~~	~~4-5~~	~~"Water came to Tanakko Bibi's house"~~	~~9 m~~	~~1.6 km~~	~~2~~
~~Ganj Baksh~~	~~14-15~~	~~"Tsunami destroyed houses, boats, and debris nearly as far inland as Parhag. Many houses and boats were stranded beside Jaddi Hill."~~	~~8 m~~	~~360 m to 1.52 km~~	~~3~~
~~Khudai Dost~~	~~10-15~~	~~"Part of Wadsar was drowned"~~			~~4~~
~~Qadir Baksh~~	~~15~~	~~"Tsunami water came to Daragah (Shrine) and then receded back. There were already scattered bivalve shells on the inundated land, but the concentration had increased after the 1945 tsunami"~~	~~10 m~~	~~1.6 km~~	~~5~~
~~Field work~~		~~The above reported localities were identified in the field. We traced a curvilinear deposit of broken bivalve (shell bed) connecting these above-mentioned localities and interpreted it to be reworked deposits from the 1945 tsunami (tsunamites).~~	~~8 m~~	~~0.3 – 1.8 km~~	~~6,7,8~~
~~*-Witness aged 4-5 years to remember the tsunami is doubtful. Most likely she repeats what she is told by others~~					

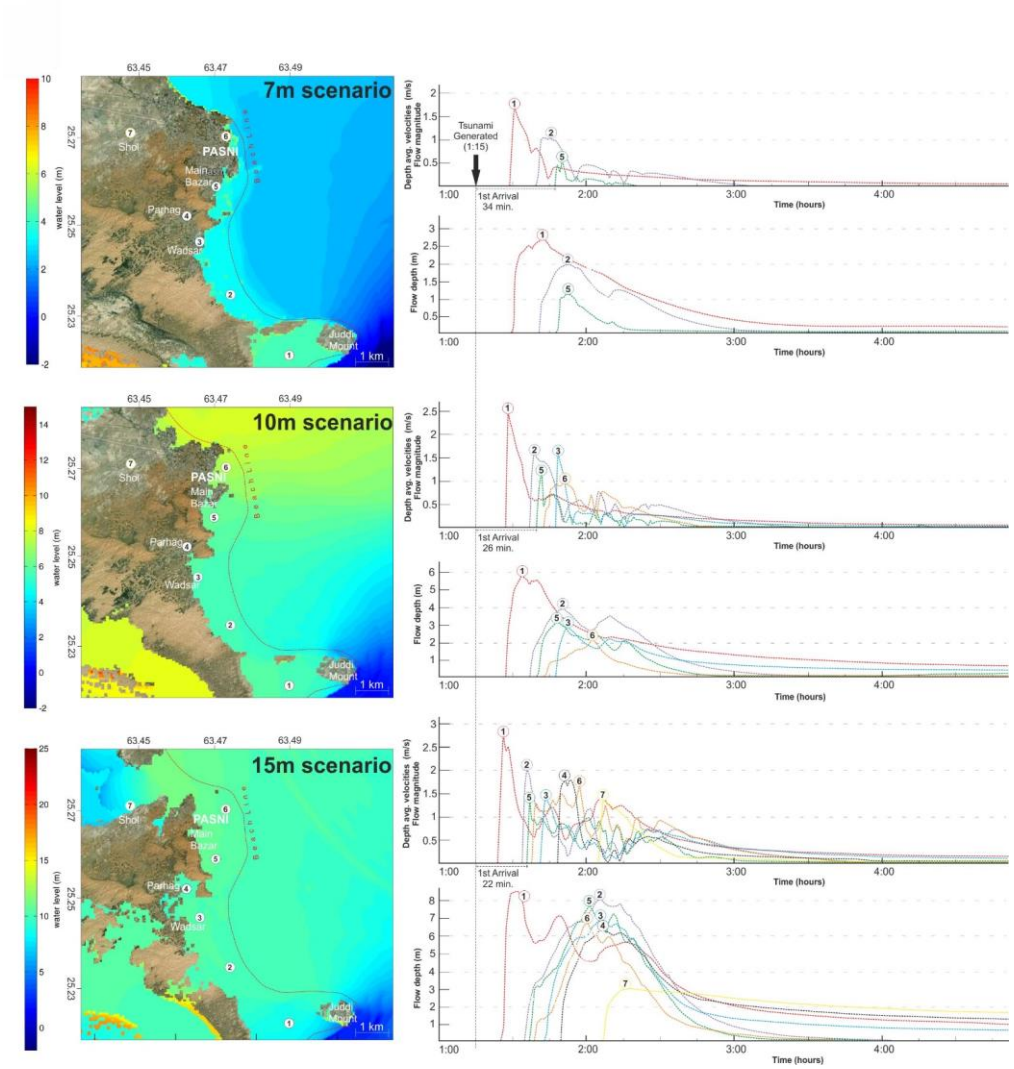

Figure 2: Hydrodynamic modelling results of each scenario with maximum inundation limits and depths at Pasni and surrounding areas. The graphs illustrate the flow depth and magnitude at monitoring points (M1 to M7). Simulation details for each scenario are provided in the supplementary materials.

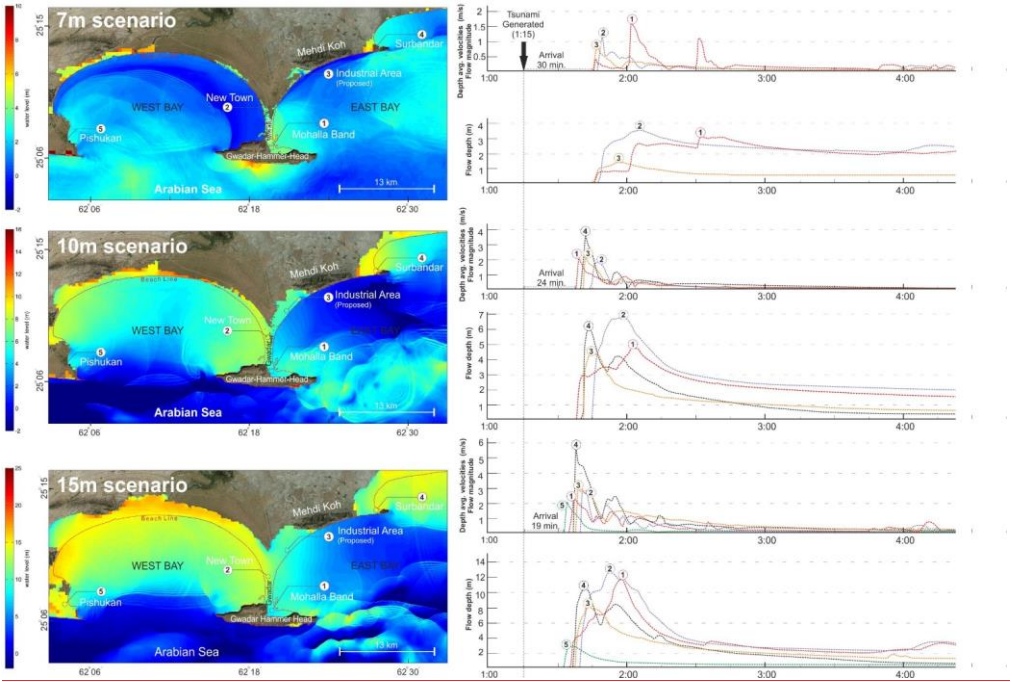

Figure 3: Hydrodynamic modelling results of each scenario with maximum inundation limits and depths at Gwadar and surrounding areas. The graphs illustrate the flow depth and magnitude at monitoring points (M1 to M5). Simulation details for each scenario are provided in the supplementary materials.

Table 3: Summarised methodology with the respective basic components used in each model.

Approach	Model	Equation/s	Reference
~~Static~~	~~**Standing wave**~~ ~~• mass conservation~~ ~~• surface roughness~~	$Head_{loss} = \left(\frac{167n^2}{\frac{1}{V_0^3}}\right) + 5\sin\ \sin\ s_0$ ~~(i)~~ $Inundation_{max} = \frac{Y_0}{Head_{loss}} 10$ ~~(ii)~~ ~~n: roughness coefficient~~ ~~s_0: Topographic slope (radian)~~ ~~Y_0: Initial wave height on the shoreline~~	~~(Berryman, 2005)~~ ~~(Prasojo et al., 2017)~~ ~~(Juniansah et al., 2018)~~ ~~(Steinritz et al., 2021)~~

Hydrodynamic	**Delft3D** • mass conservation • momentum eq. • surface roughness • simulations	• *Hydrodynamic equations* • *Continuity equation* • *Momentum equations in horizontal direction* • *Vertical velocities* • *Hydrostatic pressure assumption* • *Coriolis force and Reynolds stresses equations* * For details, referred to (Deltares, 2017), pp. 175–181)	(Deltares, 2017) (Gelfenbaum et al., 2007) (Chacón-Barrantes et al., 2013) (Röbke et al., 2016) (Röbke et al., 2018) (Van Ormondt et al., 2020) (Sujatmiko et al., 2023)

645

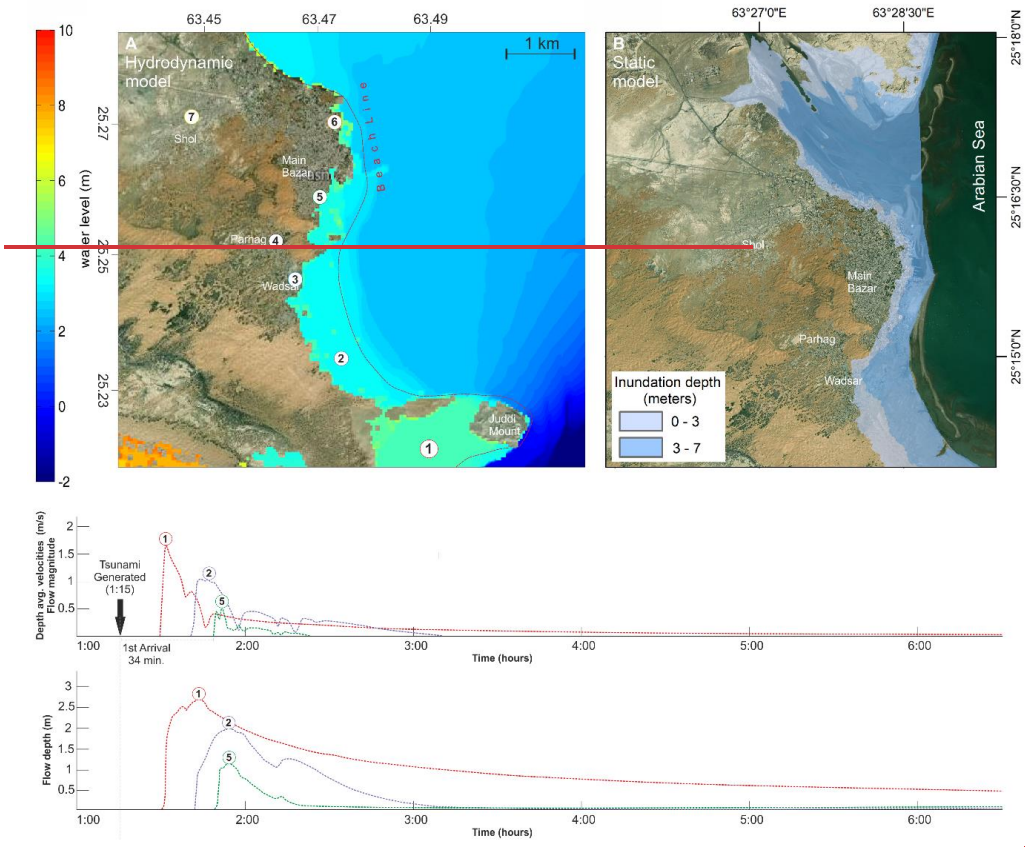

Figure 2 (Scenario 7 m): A Hydrodynamic modelling results of maximum inundation limits and depths at Pasni and surrounding areas (Supplements: Simulations 2 Pasni 7 m scenario). The graphs show the flow depth and flow magnitude at each monitoring point (M1 to M7). B Static modelling results showing flow depths and inundation extents.

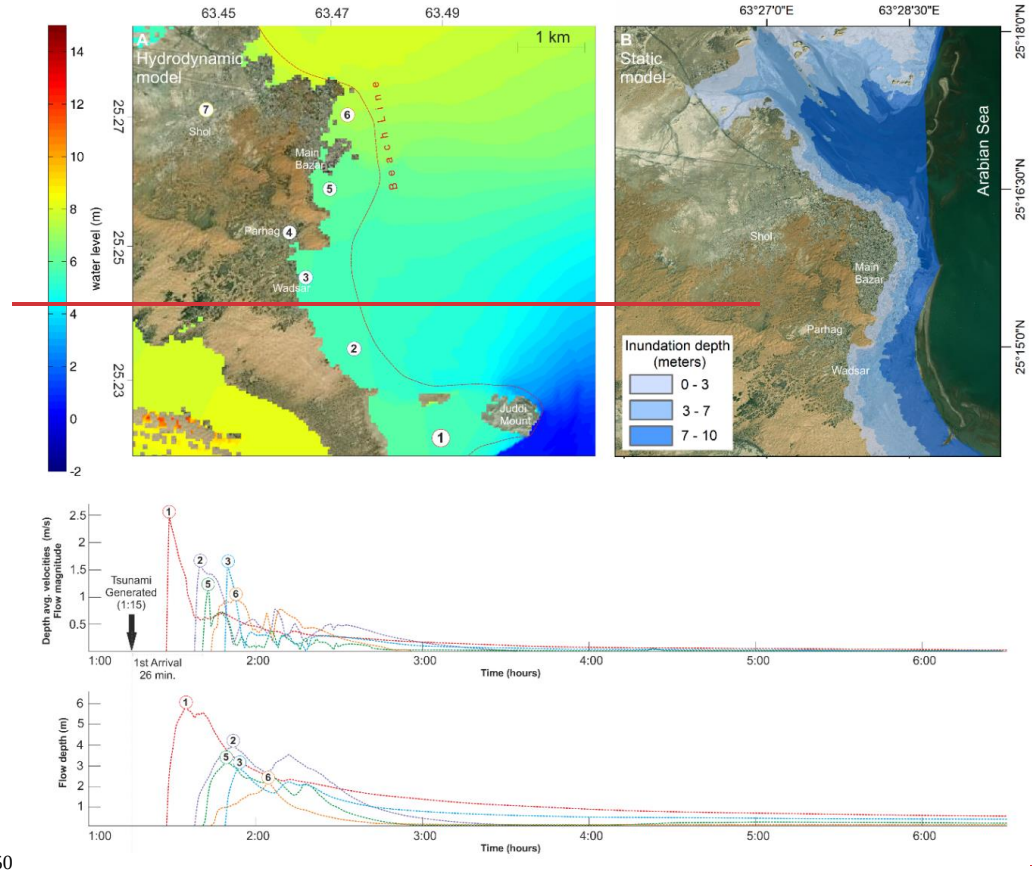

650 **Figure 3 (Scenario 10 m): A Hydrodynamic modelling results of maximum inundation limits and depths at Pasni and surrounding areas (Supplements: Simulations-3 Pasni 10 m scenario). The graphs show the flow depth and flow magnitude at each monitoring point (M1 to M7). B Static modelling results show flow depths and inundation extents.**

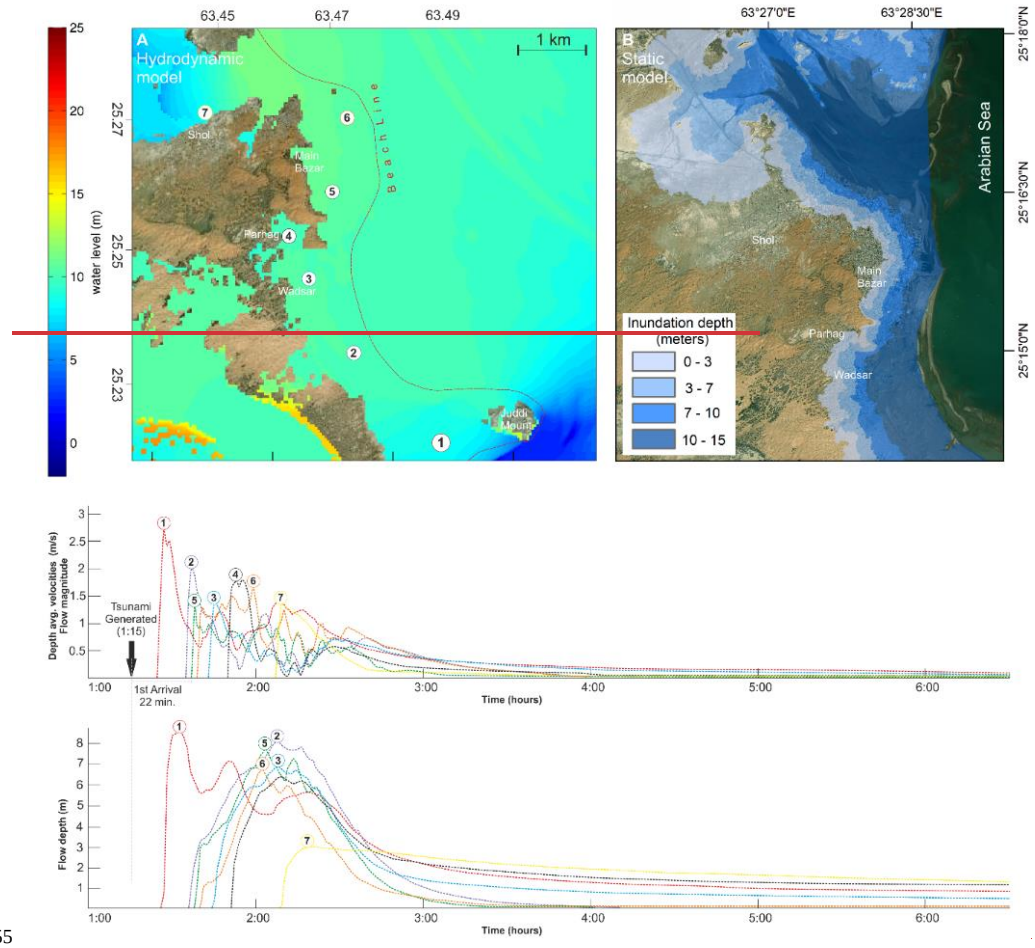

Figure 4 (Scenario 15 m): A Hydrodynamic modelling results of maximum inundation limits and depths at Pasni and surrounding areas (Supplements: Simulations 4 Pasni 15 m scenario). The graphs show the flow depth and flow magnitude at each monitoring point (M1 to M7). B Static modelling results showing flow depths and inundation extents.

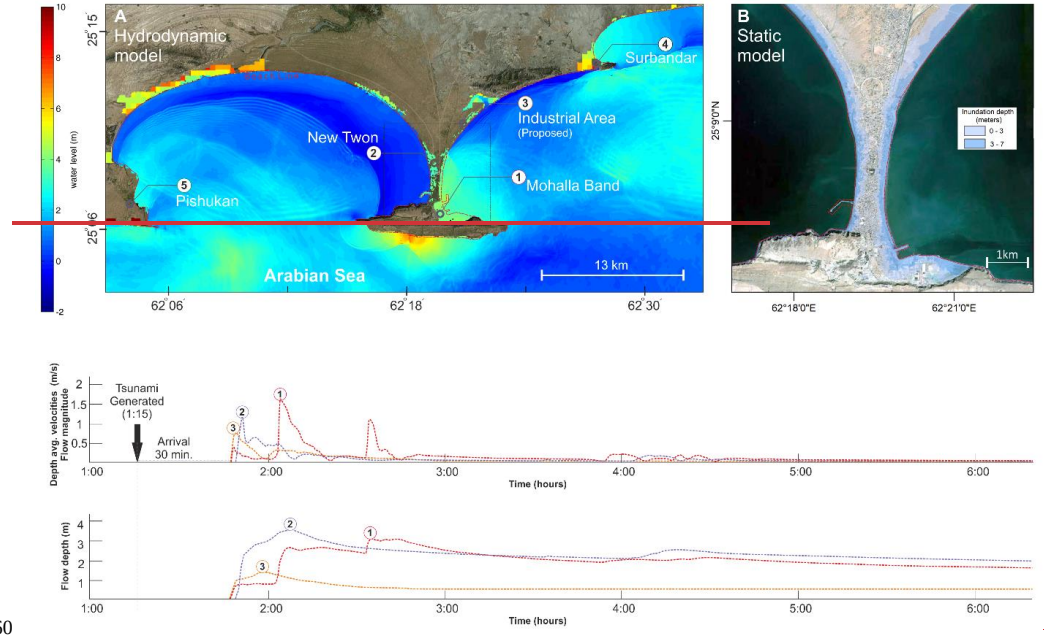

Figure 5 (Scenario 7 m): A Hydrodynamic modelling results of maximum inundation limits and depths at Pasni and surrounding areas (Supplements: Simulations-6 Gwadar 7 m scenario). The graphs show the flow depth and flow magnitude at each monitoring point (M1 to M7). B Static modelling results showing flow depths and inundation extents.

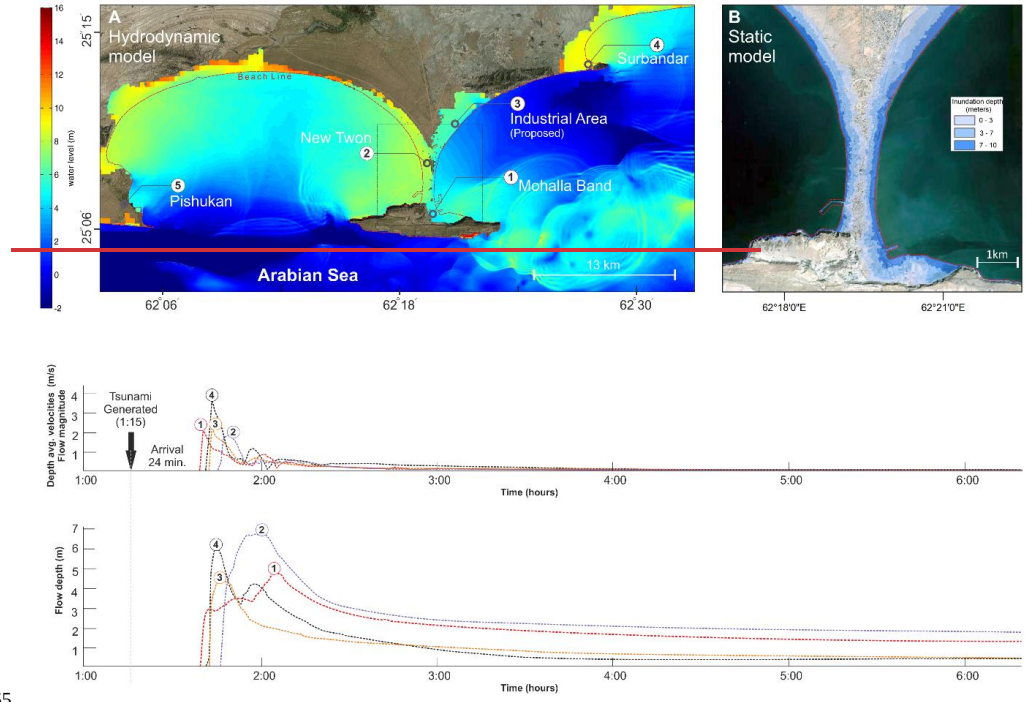

665 **~~Figure 6 (Scenario 10 m): A Hydrodynamic modelling results of maximum inundation limits and depths at Pasni and surrounding areas (Supplements: Simulations 7 Gwadar 10 m scenario). The graphs show the flow depth and flow magnitude at each monitoring point (M1 to M7). B Static modelling results showing only flow depths and inundation extents.~~**

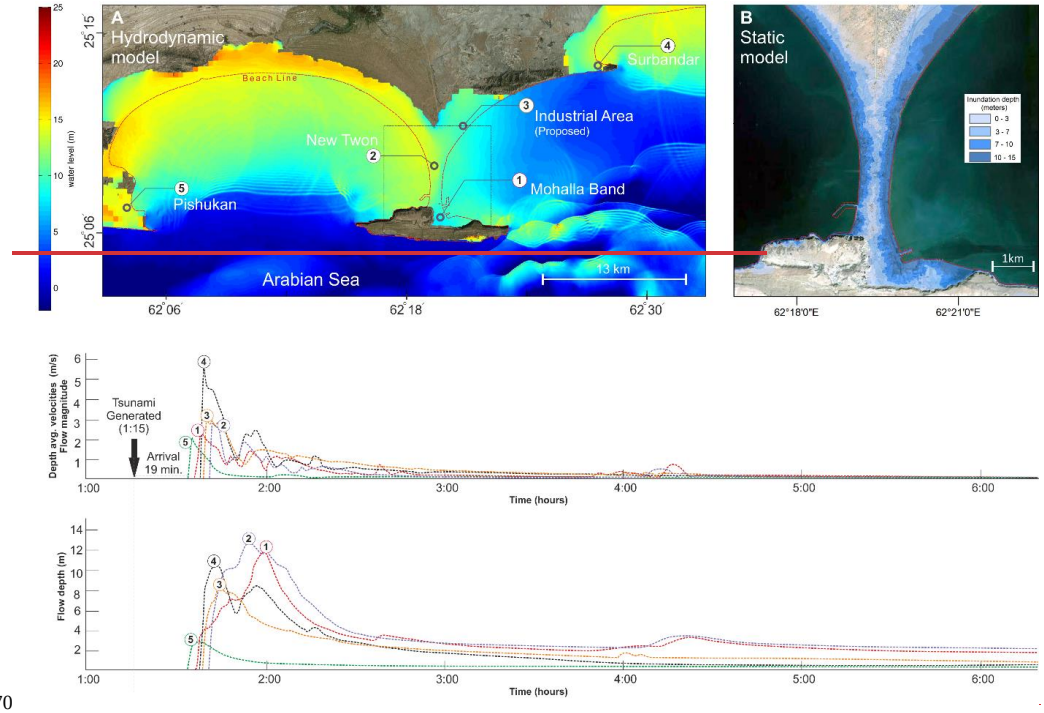

Figure 7 (Scenario 15 m): A Hydrodynamic modelling results of maximum inundation limits and depths at Pasni and surrounding areas (Supplements: Simulations 8 Gwadar 15 m scenario). The graphs show the flow depth and flow magnitude at each monitoring point (M1 to M7). B Static modelling results showing flow depths and inundation extents.

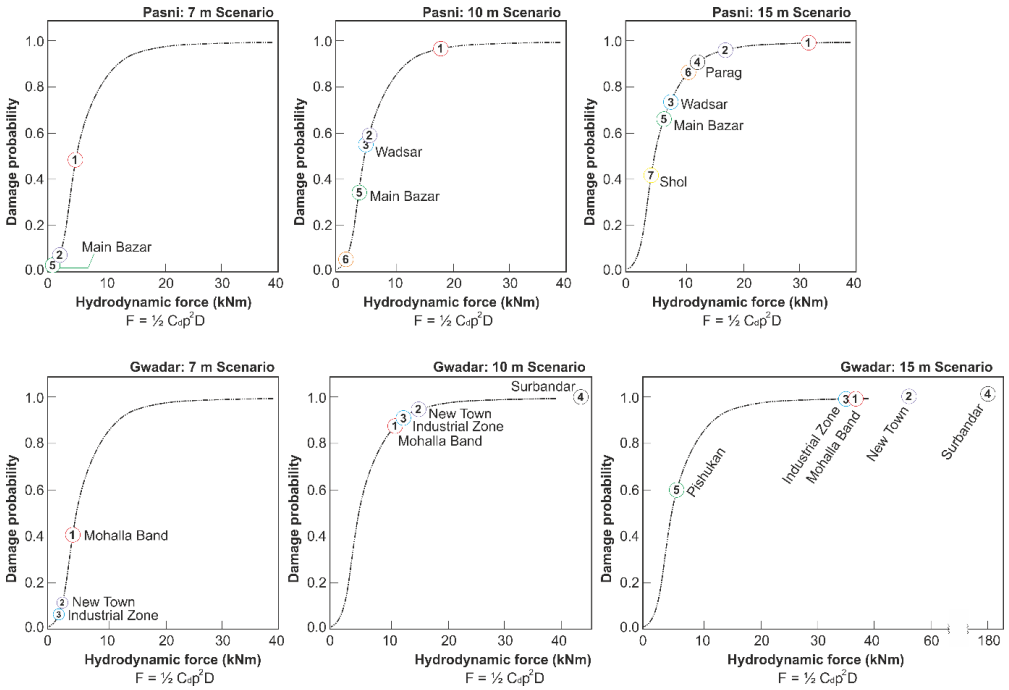

675 **Figure 8: A Probability structural damage plotted against the hydrodynamic force at each monitoring point. Top row: Pasni, Bottom row: Gwadar. The results plotted on fragility curves developed by (Koshimura et al., 2009).**

680 **~~Table 4: Table showing compilation of reporting wave heights and times at Pasni, Karachi and Mumbai. The line-graphs below compare the observed arrival times with the modelled one at Karachi and Mumbai (Revised after Heidarzadeh and Satake, (2014b). The references not in the text (Heidarzadeh et al., 2008, 2009), (Jaiswal et al., 2009)~~**

~~Reference~~	~~Observed Max. Wave height (location)~~	~~Observed arrival time of wave/s (1st, 2nd, 3rd)~~	~~Arrival time/delay~~
~~(Pendse, 1946)~~	~~12-15 m (Pasni)~~	~~04:00, 07:15, --~~	~~"At about 4:00 IST a wave was noticed but it did not come inland. At about 7:15 IST another wave swept over the town and caused widespread havoc. The height of this wave has been estimated variously from 40 ft to 60 ft (~12 m to 18 m)"~~
	~~1.4 m (Karachi)~~	~~05:30, 07:00, 07:50~~	~~last wave was highest with wave height of 1.4 m~~
	~~1.9 m (Mumbai)~~	~~08:15, --, --~~	
~~(Gates et al.,~~	~~7-10 m (Pasni)~~	~~04:00, 04:30, 5:00~~	

1977)			
(Page et al., 1979)	7-10 m (Pasni)	04:30, 05:00, --	"Local inhabitants report that three tsunamis hit the Makran Coast 1.5 to 2 hours (4:30, 5:00 IST). Field investigation showed that there was no uplift of Pasni resulting from the earthquake, but the Ormara area rose about 2 m"
(Neetu et al., 2011)	0.28 m (Karachi)	05:00, --, --	Karachi Tide Gauge (1945), First wave arrival 5:00 IST
	0.35 m (Mumbai)	08:09, --, --	Mumbai Tide Gauge (1945), First wave arrival 08:09 IST
(Kakar et al., (2014)	≥7 m (Pasni)	04:00, --, --	Three waves with interval of few minutes arrived ~30 minutes after the earthquake, Interviewees: i) Khuadi Dost, ii) Sakhi iii) Daad, Madni

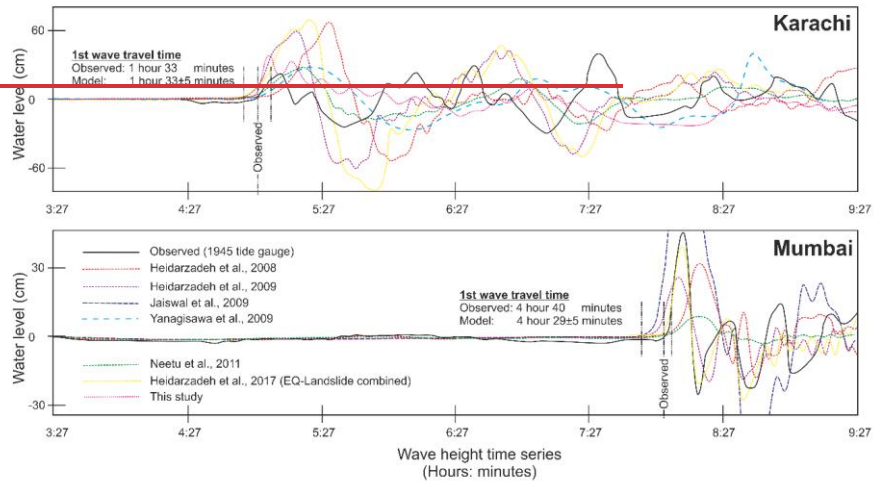

685

690

695